Optical nonlocality induced *Zitterbewegung* near the Dirac point in metal-dielectric multilayer metamaterials

Lei Sun,[1] **Jie Gao,**[2] **and Xiaodong Yang**[3]

[1]*Department of Mechanical and Aerospace Engineering, Missouri University of Science and Technology, Rolla, Missouri 65409, USA*
[2]*gaojie@mst.edu*
[3]*yangxia@mst.edu*

Abstract: The optical nonlocality near the Dirac point in infinite periodic metal-dielectric multilayer metamaterials is investigated through the dispersion relation analysis according to the transfer-matrix method. It is revealed that both the symmetric and asymmetric surface plasmon polariton modes present the zero nonlocal effective permittivity, and the degeneracy of these two modes results in the emergence of the Dirac point. Furthermore, the *Zitterbewegung* effect near the Dirac point induced by the optical nonlocality is demonstrated due to the coherent coupling between the symmetric and asymmetric modes.

© 2016 Optical Society of America

OCIS codes: (160.3918) Metamaterials; (310.4165) Multilayer design; (260.2030) Dispersion; (310.6628) Subwavelength structures, nanostructures.

References and links

1. H. Shin and S. Fan, "All-angle negative refraction and evanescent wave amplification using one-dimensional metallodielectric photonic crystals," Appl. Phys. Lett. **89**, 151102 (2006).
2. X. Fan, G. P. Wang, J. C. W. Lee, and C. T. Chan, "All-angle broadband negative refraction of metal waveguide arrays in the visible range: theoretical analysis and numerical demonstration," Phys. Rev. Lett. **97**, 073901 (2006).
3. L. Verslegers, P. B. Catrysse, Z. Yu, and S. Fan, "Deep-subwavelength focusing and steering of light in an aperiodic metallic waveguide array," Phys. Rev. Lett. **103**, 033902 (2009).
4. G. Bartal, G. Lerosey, and X. Zhang, "Subwavelength dynamic focusing in plasmonic nanostructures using time reversal," Phys. Rev. B **79**, 201103 (2009).
5. L. Sun, S. Feng, and X. Yang, "Loss enhanced transmission and collimation in anisotropic epsilon-near-zero metamaterials," Appl. Phys. Lett. **101**, 241101 (2012).
6. Y. He, L. Sun, S. He, and X. Yang, "Deep subwavelength beam propagation in extremely loss-anisotropic metamaterials," J. Opt. **15**, 055105 (2013).
7. L. Sun, X. Yang, W. Wang, and J. Gao, "Diffraction-free optical beam propagation with near-zero phase variation in extremely anisotropic metamaterials," J. Opt. **17**, 035101 (2015).
8. X. Yang, J. Yao, J. Rho, X. Yin, and X. Zhang, "Experimental realization of three-dimensional indefinite cavities at the nanoscale with anomalous scaling laws," Nat. Photonics **6**, 450–454 (2012).
9. J. Zhao, H. Zhang, X. Zhang, D. Li, H. Lu, and M. Xu, "Abnormal behaviors of Goos-Hänchen shift in hyperbolic metamaterials made of aluminum zinc oxide materials," Photon. Res. **1**, 160–163 (2013).
10. J. Elser, V. A. Podolskiy, I. Salakhutdinov, and I. Avrutsky, "Nonlocal effects in effective-medium response of nanolayered metamaterials," Appl. Phys. Lett. **90**, 191109 (2007).
11. A. A. Orlov, P. M. Voroshilov, P. A. Belov, and Y. S. Kivshar, "Engineered optical nonlocality in nanostructured metamaterials," Phys. Rev. B **84**, 045424 (2011).
12. S. Feng, J. M. Elson, and P. L. Overfelt, "Optical properties of multilayer metal-dielectric nanofilms with all-evanescent modes," Opt. Express **13**, 4113–4124 (2005).

#256788 Received 4 Jan 2016; revised 19 Feb 2016; accepted 17 Mar 2016; published 23 Mar 2016
© 2016 OSA

13. K. Sakoda, "Universality of mode symmetries in creating photonic Dirac cones," J. Opt. Soc. Am. B **29**, 2770–2778 (2012).
14. X. Huang, Y. Lai, Z. H. Hang, H. Zheng, and C. T. Chan, "Dirac cones induced by accidental degeneracy in photonic crystals and zero-refractive-index materials," Nat. Mater. **10**, 582–586 (2011).
15. L. Sun, J. Gao, and X. Yang, "Giant optical nonlocality near the Dirac point in metal-dielectric multilayer metamaterials," Opt. Express **21**, 21542–21555 (2013).
16. A. V. Chebykin, A. A. Orlov, A. V. Vozianova, S. I. Maslovski, Yu. S. Kivshar, and P. A. Belov, "Nonlocal effective medium model for multilayered metal-dielectric metamaterials," Phys. Rev. B **84**, 115438 (2011).
17. A. V. Chebykin, A. A. Orlov, C. R. Simovski, Yu. S. Kivshar, and P. A. Belov, "Nonlocal effective parameters of multilayered metal-dielectric metamaterials," Phys. Rev. B **86**, 115420 (2012).
18. L. Sun, Z. Li, T. S. Luk, X. Yang, and J. Gao, "Nonlocal effective medium analysis in symmetric metal-dielectric multilayer metamaterials," Phys. Rev. B **91**, 195147 (2015).
19. X. Zhang, "Observing *Zitterbewegung* for photons near the Dirac point of a two-dimensional photonic crystal," Phys. Rev. Lett. **100**, 113903 (2008).
20. L.-G. Wang, Z.-G. Wang, and S.-Y. Zhu, "Zitterbewegung of optical pulses near the Dirac point inside a negative-zero-positivie index metamaterial," Europhys. Lett. **86**, 47008 (2009).
21. W. Cai and V. Shalaev, *Optical Metamaterials* (Springer, 2010).
22. I. H. Malitson and M. J. Dodge, "Refractive index and birefringence of synthetic sapphire," J. Opt. Soc. Am. **62**, 1405 (1972).
23. S. H. Nam, A. J. Taylor, and A. Efimov, "Diabolical point and conical-like diffraction in periodic plasmonic nanostructures," Opt. Express **18**, 10120–10126 (2010).
24. K. E. Ballantine, J. F. Donegan, and P. R. Eastham, "Conical diffraction and the dispersion surface of hyperbolic metamaterials," Phys. Rev. A **90**, 013803 (2014).
25. S. H. Nam, J. Zhou, A. J. Taylor, and A. Efimov, "Dirac dynamics in one-dimensional graphene-like plasmonic crystals: pseudo-spin, chirality, and diffraction anomaly," Opt. Express **18**, 25329–25338 (2010).

1. Introduction

Metal-dielectric multilayer metamaterials have been studied for realizing many intriguing photonics applications such as negative refraction [1, 2], subwavelength focusing [3, 4], diffraction-free propagation [5–7], anomalous indefinite cavities [8], and Goos-Hänchen shifts [9]. In general, the electromagnetic properties of periodic metal-dielectric multilayer metamaterials are simplify described by the local effective medium theory (EMT), since the meta-atoms (unit cells) of the multilayers are in the scale much smaller than the wavelength. However, the dramatically different electromagnetic properties between the metal layer and the dielectric layer will cause significant variations of the electromagnetic field over the scale of meta-atom, so that strong spatial dispersion will be generated to induce the optical nonlocality [10] not considered in local EMT. In addition, the optical nonlocality in the periodic metal-dielectric multilayer stack will be significantly enhanced with the excitation of surface plasmon polariton (SPP) modes along the interface of the metal layer and the dielectric layer [11]. The coupling of SPP modes in metal-dielectric multilayer stacks will lead to many interesting electromagnetic phenomena. One example is the formation of the Dirac point first demonstrated in metal-dielectric nanofilms in [12] due to the degeneracy of the symmetric and asymmetric eigenmodes [13]. The Dirac point implies an effectively zero "optical mass" (zero electric permittivity) when located at the center of the Brillouin zone, and it is important in the research of epsilon-near-zero (ENZ) metamaterials [14, 15] and the nonlocal EMT [16–18].

In this work, the optical nonlocality near the Dirac point of the infinite periodic metal-dielectric multilayer metamaterials is further investigated. According to the transfer-matrix method, the exact dispersion relation of the periodic metal-dielectric multilayers is analyzed to reveal the existence of both the symmetric and asymmetric SPP modes, where zero nonlocal effective permittity is obtained. It is shown that the emergence of the Dirac point is due to the degeneracy of the symmetric and asymmetric SPP modes. On the other hand, the optical nonlocality of metal-dielectric multilayer stack is described by a nonlocal EMT through the study of the iso-frequency contours (IFCs). Furthermore, the strong optical nonlocality induced *Zitterbewegung* effect [19, 20] is demonstrated near the Dirac point in metal-dielectric

#256788 Received 4 Jan 2016; revised 19 Feb 2016; accepted 17 Mar 2016; published 23 Mar 2016
© 2016 OSA

multilayer stack, due to the coherent coupling between the symmetric and asymmetric SPP modes.

2. Dispersion relation analysis in metal-dielectric multilayer stack

As depicted in Fig. 1(a), a metal-dielectric multilayer stack composited of infinite alternating layers of gold (Au) and alumina (Al_2O_3) with thickness $a_m = 10\,\text{nm}$ and $a_d = 350\,\text{nm}$ is considered, with respect to the TM polarized light propagating in the x-y plane. The permittivity of Au is described by the Drude model as $\varepsilon_m = \varepsilon_\infty - \omega_p^2/\omega(\omega + i\gamma)$ with the permittivity constant $\varepsilon_\infty = 9$, the plasma frequency $\omega_p = 1.38 \times 10^{16}\,\text{rad}\cdot\text{s}^{-1}$, and the damping factor $\gamma = 0.11 \times 10^{15}\,\text{rad}\cdot\text{s}^{-1}$ [21]. In order to emphasize the optical nonlocality, the damping factor γ in the Drude model is ignored in the following theoretical analysis. The permittivity of Al_2O_3 is simplify set as $\varepsilon_d = 1.76^2$ [22].

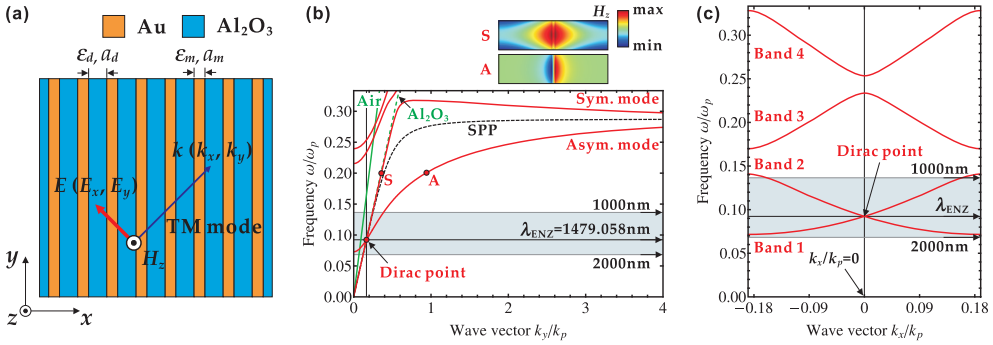

Fig. 1. (a) Schematic of the infinite periodic Au-Al_2O_3 multilayer stack with respect to the TM polarized light. (b) The dispersion relation of frequency ω/ω_p versus wave vector k_y/k_p (red-solid curves) of the Au-Al_2O_3 multilayer stack, compared with the typical SPP dispersion based on $k_y/k_p = \omega/\omega_p\sqrt{\varepsilon_m\varepsilon_d/(\varepsilon_m+\varepsilon_d)}$ (black-dashed curve). The light lines in Air (green-solid line) and in Au-Al_2O_3 (green-dashed line) are also displayed. The distributions of the magnetic field H_z for the symmetric and asymmetric modes at the point S and the point A are presented. (c) The corresponding band structure of frequency ω/ω_p versus wave vector k_x/k_p with the Dirac point at the Brillouin zone center.

According to the transfer-matrix method, the propagation of the TM polarized light in the Au-Al_2O_3 multilayer stack follows the dispersion relation as [15]

$$\cos\left(k_x(a_m+a_d)\right) = \cos\left(k_{mx}a_m\right)\cos\left(k_{dx}a_d\right) - \frac{1}{2}\left(\frac{\varepsilon_m k_{dx}}{\varepsilon_d k_{mx}} + \frac{\varepsilon_d k_{mx}}{\varepsilon_m k_{dx}}\right)\sin\left(k_{mx}a_m\right)\sin\left(k_{dx}a_d\right) \quad (1)$$

with $k_{mx} = (\varepsilon_m k_0^2 - k_y^2)^{1/2}$ and $k_{dx} = (\varepsilon_d k_0^2 - k_y^2)^{1/2}$. Under the condition of $k_x = 0$, Eq. (1) reveals the dispersion relation between frequency ω/ω_p and wave vector k_y/k_p of the Au-Al_2O_3 multilayer stack as

$$\cos\left(k_{mx}a_m\right)\cos\left(k_{dx}a_d\right) - \frac{1}{2}\left(\frac{\varepsilon_m k_{dx}}{\varepsilon_d k_{mx}} + \frac{\varepsilon_d k_{mx}}{\varepsilon_m k_{dx}}\right)\sin\left(k_{mx}a_m\right)\sin\left(k_{dx}a_d\right) = 1 \quad (2)$$

with the corresponding dispersion curves shown in Fig. 1(b). In the following analysis, the frequency ω and the wave vector components k_x and k_y are normalized by the plasma frequency ω_p and the related plasma wave vector $k_p = \omega_p/c$. As displayed in Fig. 1(b), the dispersion relation of $\omega/\omega_p \sim k_y/k_p$ possesses two branches below the light line in Al_2O_3, which represent

#256788 Received 4 Jan 2016; revised 19 Feb 2016; accepted 17 Mar 2016; published 23 Mar 2016
© 2016 OSA

the symmetric and asymmetric SPP modes confined at the interface of Au layer and Al_2O_3 layer. The dispersion relation implies the variations of the TM polarized light over the size of the period in the Au-Al_2O_3 multilayer stack as functions of both frequency and wave vector, leading to the optical nonlocality. The excitation of both the symmetric and asymmetric SPP modes will enhance the variation of the electromagnetic field over the scale of the multilayer period, as the electromagnetic field is strongly confined at the interface of Au layer and Al_2O_3 layer. The magnetic field H_z distributions of the symmetric and asymmetric SPP modes at the point S and the point A are also presented in Fig. 1(b). As the wave vector k_y/k_p increases, the two SPP branches converge to the typical SPP mode as $k_y/k_p = \omega/\omega_p\sqrt{\varepsilon_m\varepsilon_d/(\varepsilon_m+\varepsilon_d)}$ due to the surface plasmon resonance, where $\varepsilon_m+\varepsilon_d=0$. Furthermore, at the position of

$$\begin{cases} k_x/k_p = 0 \\ k_y/k_p = \sqrt{\varepsilon_d a_m a_d/\left((a_d-a_m)(\varepsilon_\infty a_m+\varepsilon_d a_d)\right)} \\ \omega/\omega_p = \sqrt{a_m/(\varepsilon_\infty a_m+\varepsilon_d a_d)} \end{cases} \tag{3}$$

the degeneracy of the symmetric and asymmetric SPP mode forms the Dirac point, at the frequency of local ENZ, where $\varepsilon_y^{\mathrm{loc}} = (\varepsilon_m a_m+\varepsilon_d a_a)/(a_m+a_d)=0$. Correspondingly, Fig. 1(c) displays the band structure of the Au-Al_2O_3 multilayer stack based on Eq. (1) under the condition of $k_y/k_p = \sqrt{\varepsilon_d a_m a_d/\left((a_d-a_m)(\varepsilon_\infty a_m+\varepsilon_d a_d)\right)}$. The band 1 and band 2 are associated with the symmetric and asymmetric SPP modes, and the degeneracy of the two modes at the Brillouin zone center ($k_x/k_p=0$) forms the Dirac point.

3. Optical nonlocality induced *Zitterbewegung* effect

The optical nonlocality in the Au-Al_2O_3 multilayer stack can be analyzed through the nonlocal EMT, where the multilayer stack is regarded as bulk nonlocal effective medium with the nonlocal effective permittivity depending on both frequency and wave vector. With respect to the infinite Au-Al_2O_3 multilayer stack, the nonlocal EMT can be introduced as follows. According to the dispersion relation of Eq. (1), the wave vector k_x can be represented as a function of frequency ω and wave vector k_y

$$k_x(\omega,k_y) = \frac{\arccos\left[\cos(k_{mx}a_m)\cos(k_{dx}a_d) - \frac{1}{2}\left(\frac{\varepsilon_m k_{dx}}{\varepsilon_d k_{mx}}+\frac{\varepsilon_d k_{mx}}{\varepsilon_m k_{dx}}\right)\sin(k_{mx}a_m)\sin(k_{dx}a_d)\right]}{a_m+a_d}. \tag{4}$$

On the other hand, the nonlocal effective medium dispersion relation of the Au-Al_2O_3 multilayer stack can be written as

$$k_x^2/\varepsilon_y^{\mathrm{nloc}} + k_y^2/\varepsilon_x^{\mathrm{nloc}} = k_0^2 \tag{5}$$

with the nonlocal effective permittivity components of $\varepsilon_x^{\mathrm{nloc}}$ and $\varepsilon_y^{\mathrm{nloc}}$

$$\begin{cases} \varepsilon_x^{\mathrm{nloc}}(\omega,k_y) = \varepsilon_x^{\mathrm{loc}} = \varepsilon_m\varepsilon_d(a_m+a_d)/(\varepsilon_m a_d+\varepsilon_d a_m) \\ \varepsilon_y^{\mathrm{nloc}}(\omega,k_y) = k_x(\omega,k_y)^2/\left[k_0^2 - k_y^2/\varepsilon_x^{\mathrm{nloc}}(\omega,k_y)\right] \end{cases} \tag{6}$$

by substituting Eq. (4) into Eq. (5). It is noted that $\varepsilon_x^{\mathrm{nloc}}$ is approximated as the local value of $\varepsilon_x^{\mathrm{loc}}$ due to the relatively weak nonlocal effects along the x-direction. In contrast to the local EMT, Eq. (6) indicates that $\varepsilon_y^{\mathrm{nloc}}=0$ when $k_x(\omega,k_y)=0$, which indicates that in Fig. 1(b) both the symmetric and asymmetric SPP branches (including the Dirac point) present the zero nonlocal effective permittivity. It can be explained that the symmetric and asymmetric SPP

#256788 Received 4 Jan 2016; revised 19 Feb 2016; accepted 17 Mar 2016; published 23 Mar 2016
© 2016 OSA

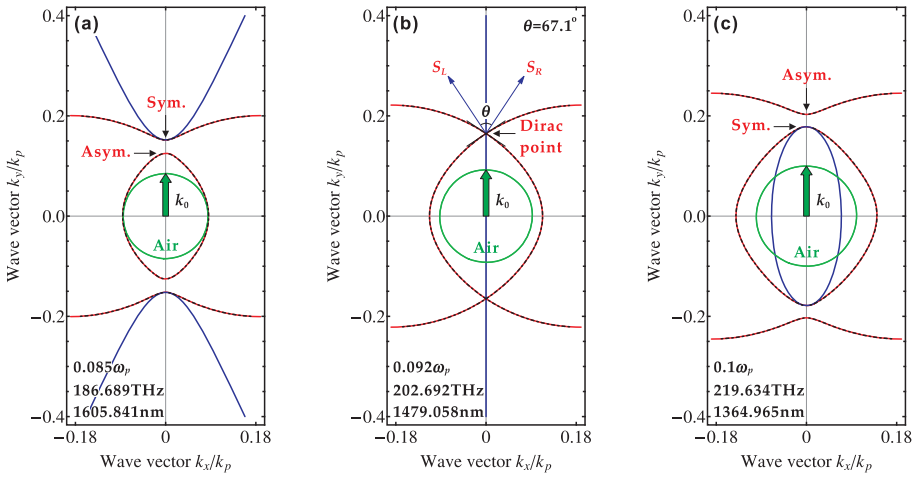

Fig. 2. The IFCs based on the dispersion relation of Eq. (1) (red-solid curves), the nonlocal effective permittivities of Eq. (6) (black-dashed curves), and the local effective permittivities (blue-solid curves) with respect to the frequency (a) $0.085\omega_p$ as 186.689 THz (below the Dirac point), (b) $0.092\omega_p$ as 202.692 THz (at the Dirac point), and (c) $0.1\omega_p$ as 219.634 THz (above the Dirac point). The IFCs of air are plotted in green circles for reference.

modes perform as evanescent waves with zero phase variation along the *x*-direction, leading to the zero nonlocal effective permittivity for both the SPP modes.

Figure 2 displays the IFCs of the Au-Al_2O_3 multilayer stack based on the dispersion relation of Eq. (1), the nonlocal effective permittivity of Eq. (6), and the local effective permittivity with the frequency below the Dirac point [Fig. 2(a)], at the Dirac point [Fig. 2(b)], and above the Dirac point [Fig. 2(c)]. Clearly, the IFCs based on Eq. (1) and Eq. (6) are exactly the same around the Dirac point, while the IFCs based on the local effective permittivity can only approximately predict the dispersion of the Au-Al_2O_3 multilayer stack close to the Brillouin zone center for the symmetric SPP mode. In particular, the IFCs based on the local effective permittivity reduce to a straight line at the frequency of Dirac point, which is dramatically different from the exact IFCs based on the nonlocal effective permittivity of Eq. (6), due to the giant optical nonlocality at the Dirac point. Moreover, the exact IFCs present a band transition for the symmetric and asymmetric SPP modes across the Dirac point. It is shown that the symmetric mode switches from a higher wave vector to a lower wave vector as the frequency increases across the Dirac point, while the asymmetric mode behaves oppositely.

Such band transition and eigenmode switching near the Dirac point will induce extraordinary beam propagation phenomena. Figure 3 shows the simulated beam propagation of a TM polarized light in terms of a Gaussian beam as $H_z = H_0 \exp(-x^2/w_0^2)$ with the frequency below the Dirac point [Fig. 3(a)], at the Dirac point [Fig. 3(b)], and above the Dirac point [Fig. 3(c)], with respect to the exact IFCs in Fig. 2. The waist of the Gaussian beam is set as $w_0 = 2\lambda$, where λ is the free space wavelength. The beam propagation patterns is plotted as the distributions of the normalized magnetic field intensity $|H_z|$. In Fig. 3(b), as the symmetric and asymmetric SPP modes degenerate at the Dirac point, the Gaussian beam splits into two beams in the multilayer stack with an angle of $\theta = 67.1°$, as predicted by the IFCs in Fig. 2(b). The beam splitting phenomenon can be explained in the context of classical conical diffraction [23, 24]. On the other hand, in Figs. 3(a) and 3(c), the beam propagation in the multilayer stack shows oscillation patterns at the frequency either below or above the Dirac point, indicating the

#256788 Received 4 Jan 2016; revised 19 Feb 2016; accepted 17 Mar 2016; published 23 Mar 2016
© 2016 OSA

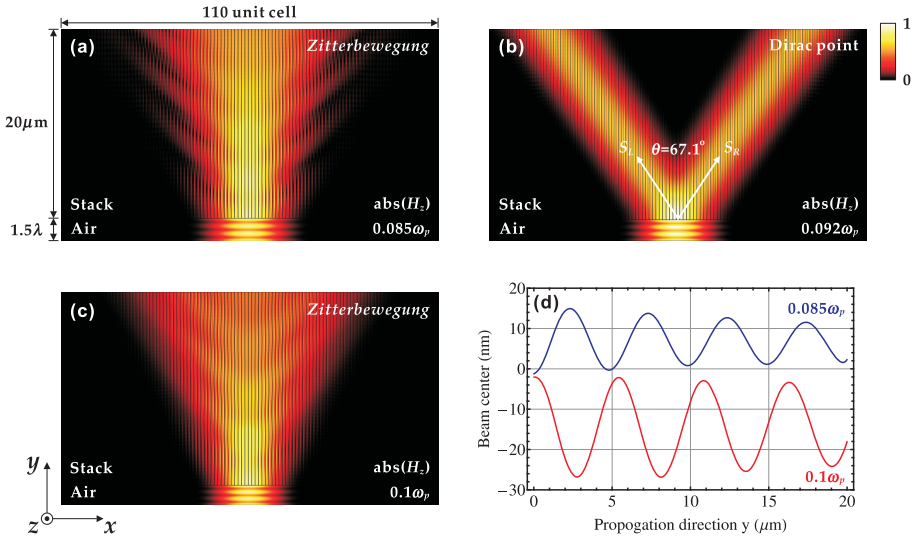

Fig. 3. The beam propagation patterns in the Au-Al_2O_3 multilayer stack for a TM polarized Gaussian beam incident from air with respect to the frequency at (a) $0.085\omega_p$ (below the Dirac point), (b) $0.092\omega_p$ (at the Dirac point), and (c) $0.1\omega_p$ (above the Dirac point) in terms of the distributions of the normalized magnetic field intensity $|H_z|$. (d) The oscillation of the beam center in the Au-Al_2O_3 multilayer stack calculated from the beam propagation patterns at the frequency of $0.085\omega_p$ (blue-solid curve) and $0.1\omega_p$ (red-solid curve) indicates the *Zitterbewegung* effect around the Dirac point.

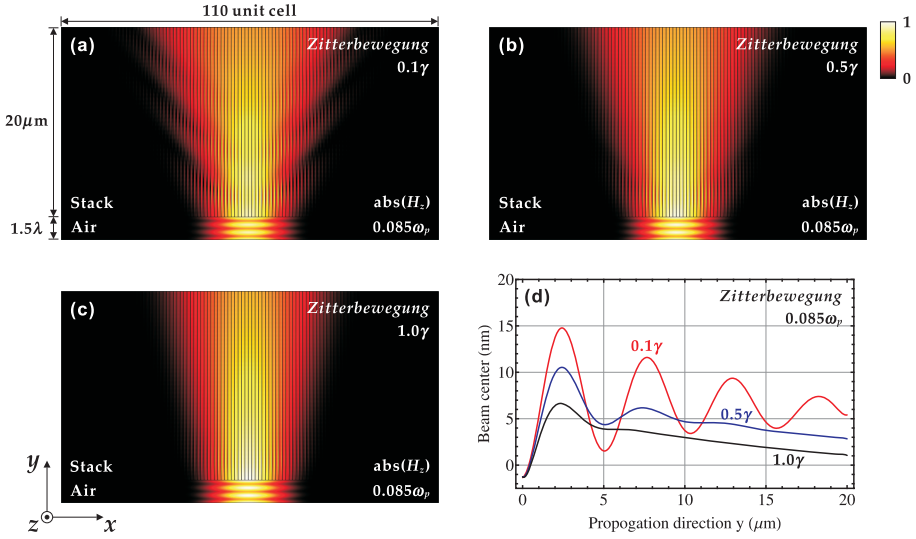

Fig. 4. The beam propagation patterns of the *Zitterbewegung* in the Au-Al_2O_3 multilayer stack for a TM polarized Gaussian beam at the frequency of $0.085\omega_p$ (below the Dirac point) with respect to different Au damping factors of (a) 0.1γ, (b) 0.5γ, and (c) 1.0γ in terms of the distributions of the normalized magnetic field intensity $|H_z|$. (d) The oscillation of the beam center in the Au-Al_2O_3 multilayer stack calculated from the beam propagation patterns with respect to different Au damping factors of 0.1γ (red-solid curve), 0.5γ (blue-solid curve), and 1.0γ (black-solid curve).

#256788
Received 4 Jan 2016; revised 19 Feb 2016; accepted 17 Mar 2016; published 23 Mar 2016
© 2016 OSA

Zitterbewegung effect due to the back-and-forth coherent coupling between the symmetric and asymmetric SPP modes [25]. The variation of the beam center shown in Fig. 3(d) defined as $x_c = \int x|H_z(x,y)|\,dx / \int |H_z(x,y)|\,dx$, clearly reveals a fast beam oscillation in the x-direction as the beam propagated along the y-direction. Since the *Zitterbewegung* effect is related to the coherent coupling between the symmetric and asymmetric SPP modes, the oscillation of the beam center also represents the band transition around the Dirac point as illustrated in Figs. 2(a) and 2(c). According to the nonlocal IFCs displayed in Figs. 2(a) and 2(c), there are only two eigenmodes, the symmetric and asymmetric SPP modes, existing in the beam propagation patterns of the *Zitterbewegung*. It is noted that the curvatures of these two eigenmodes present opposite values near the $k_x/k_p = 0$ region. This fact indicates that as the beam propagating along y-direction, the beam diffraction angle will oscillate back and forth between a positive value and a negative value, corresponding to the coherent coupling between the symmetric and asymmetric SPP modes. The oscillation of beam diffraction finally leads to the observed *Zitterbewegung* effect shown in Figs. 3(a) and 3(c). As the frequency is below the Dirac point, the symmetric SPP mode has higher wave vector k_y than the asymmetric SPP mode, resulting in the beam center oscillation in the positive region of the x-coordinate. On the contrary, after the band transition across the Dirac point at a higher frequency, the asymmetric SPP mode gets higher wave vector k_y than the symmetric SPP mode, which flips the beam center oscillation to the negative region of the x-coordinate.

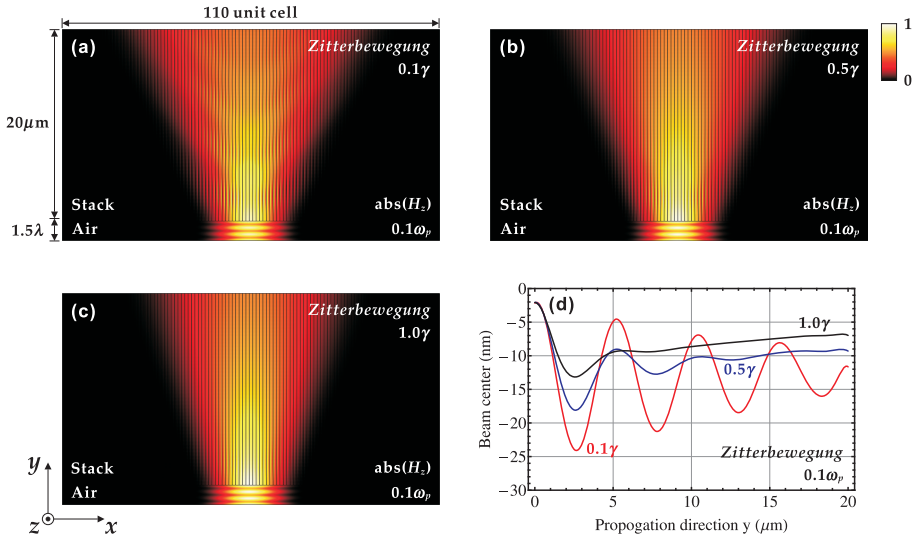

Fig. 5. The beam propagation patterns of the *Zitterbewegung* in the Au-Al_2O_3 multilayer stack for a TM polarized Gaussian beam at the frequency of $0.1\omega_p$ (above the Dirac point) with respect to different Au damping factors of (a) 0.1γ, (b) 0.5γ, and (c) 1.0γ in terms of the distributions of the normalized magnetic field intensity $|H_z|$. (d) The oscillation of the beam center in the Au-Al_2O_3 multilayer stack calculated from the beam propagation patterns with respect to different Au damping factors of 0.1γ (red-solid curve), 0.5γ (blue-solid curve), and 1.0γ (black-solid curve).

In the previous analysis, the Au damping factor γ in the Drude model is neglected to enhance the effects of optical nonlocality in the Au-Al_2O_3 multilayer stack. However, the optical loss of Au will affect the oscillation strength of the *Zitterbewegung* effect. As shown in Fig. 4, the beam propagation patterns of the *Zitterbewegung* in the Au-Al_2O_3 multilayer stack are simulated at the frequency of $0.085\omega_p$ below the Dirac point with respect to different Au damping factors

#256788 Received 4 Jan 2016; revised 19 Feb 2016; accepted 17 Mar 2016; published 23 Mar 2016
© 2016 OSA

of 0.1γ [Fig. 4(a)], 0.5γ [Fig. 4(b)], and 1.0γ [Fig. 4(c)]. It is clearly shown that the beam oscillation strength of the *Zitterbewegung* in the Au-Al_2O_3 multilayer stack is significantly suppressed by the Au damping factor. Figure 4(d) plots the corresponding oscillations of the beam center for different Au damping factors, indicating the reduced oscillation amplitude due to the influence of the optical loss. Nevertheless, the *Zitterbewegung* effect can still be observed in the simulation even as the optical loss of metal goes up to 1.0γ. Furthermore, similar simulation results are obtained for the frequency of $0.1\omega_p$ above the Dirac point, as displayed in Fig. 5. Moreover, according to the comparison on the beam center oscillations for different Au damping factors in Figs. 3(d), 4(d), and 5(d), it is demonstrated that the Au damping factor will not affect the band transition for the symmetric and asymmetric SPP modes across the Dirac point in the *Zitterbewegung*, manifesting the flipping of the beam center oscillations from the positive region to the negative region of the *x*-coordinate as the beam switches from a lower frequency to a higher frequency across the Dirac point.

4. Conclusions

The optical nonlocality near the Dirac point in infinite periodic metal-dielectric multilayer metamaterials has been investigated by performing the dispersion relation analysis based on the transfer-matrix method. It is shown that the degeneracy of the symmetric and asymmetric SPP modes forms the Dirac point where giant optical nonlocality exists. Both the symmetric and asymmetric SPP modes in the dispersion curves present the zero nonlocal effective permittivity. With the nonlocal EMT analysis, exact IFCs have been studied near the Dirac point, leading to the extraordinary beam propagation of the *Zitterbewegung* effect in the multilayer stack. Furthermore, it is demonstrated that the *Zitterbewegung* effect induced by the optical nonlocality is due to the coherent coupling between the symmetric and asymmetric SPP modes. *Zitterbewegung* is originally related to the trembling oscillation motion of a free Dirac electron due to the coherent coupling between the positive and negative energy states. The demonstration of the optical *Zitterbewegung* effect in metal-dielectric multilayer metamaterials due to the coupling between the symmetric and asymmetric SPP eigenmodes open new opportunities in exploring many complex quantum phenomena of nonrelativistic and relativistic electrons in condensed-matter physics, such as Bloch oscillations, Zener tunneling, and Klein tunneling. The analysis of the effects of metal optical loss on the beam propagation patterns of the *Zitterbewegung* further facilitates the way toward the future spatial observation of optical *Zitterbewegung* in metal-dielectric multilayer metamaterials in experiments.

Acknowledgments

The authors acknowledge support from the National Science Foundation under Grant No. DMR-1552871 and CBET-1402743, and U.S. Army Research Office Award No. W911NF-15-1-0477.

#256788 Received 4 Jan 2016; revised 19 Feb 2016; accepted 17 Mar 2016; published 23 Mar 2016
© 2016 OSA